JTTEE5 19:566–574
DOI: 10.1007/s11666-009-9423-1
1059-9630/$19.00 © ASM International

Induction Plasma Synthesis of Nano-Structured SOFCs Electrolyte Using Solution and Suspension Plasma Spraying: A Comparative Study

Lu Jia and François Gitzhofer

(Submitted April 19, 2009; in revised form September 13, 2009)

In this paper, two plasma spraying technologies: solution plasma spraying (SolPS) and suspension plasma spraying (SPS) were used to produce nano-structured solid oxide fuel cells (SOFCs) electrolytes. Both plasma spraying processes were optimized in order to achieve the thin gas-tight electrolytes. The comparison of the two plasma spraying processes is based on electrolyte phase, microstructure, morphology, as well as on plasma deposition rate. The results show that nano-structured thin electrolytes (~5 μm thick) have been successfully SPS deposited on porous anodes with a high deposition rate. Compared to the electrolytes produced by SolPS, the SPS-deposited electrolyte layer is much denser. During the SPS process, fine droplets of 0.5-1 μm in diameter impact on the surface of the coating and penetrate into the pores of the anode. As the stresses are reduced on the resulting 0.5-2 μm splats, there is no apparent microcracks network on the splats, this resulting in highly gas-tight coatings. It is demonstrated that the SPS process is beneficial for the improvement of the performance of the films to be used as SOFC electrolytes.

Keywords nano-structured electrolyte, solid oxide fuel cells (SOFCs), solution plasma spray (SolPS), suspension plasma spray (SPS), thin film

1. Introduction

The successful introduction of solid oxide fuel cells (SOFCs) as an environmentally friendly energy converter into the highly competitive market for electric power generation depends on the development of technologies which will bring about reduction in production costs. Furthermore, development of intermediate temperature SOFCs (IT-SOFCs) that operate at temperatures of 600-750 °C is also added to the potential cost reduction (Ref 1-4). In this perspective, the problems of ohmic loss (Ref 5) and the insufficient ionic conductivity of current yttria-stabilized zirconia (YSZ) electrolytes (Ref 6) can be overcome by using alternative materials with higher ionic conductivity compared to YSZ, as well as by decreasing the electrolyte resistance by reducing its thickness to 5-10 μm.

Cation-doped ceria with a fluorite structure is one of the most suitable electrolyte candidates for IT-SOFCs. Unfortunately, these cerium (CeO_2) based oxides are known to undergo reduction at low oxygen partial pressure, and become mixed conductors (Ref 7-15). To overcome this problem and to improve the conductivity for IT-SOFCs, the influence of nano-structured features in the doped CeO_2 systems on the mixed conductivity should be taken into account (Ref 16, 17). A high density of defects in nano-structured materials provides a large number of active sites for ionic conduction and high diffusivity through nano-sized grain boundaries to promote fast kinetics and ion transportation (Ref 18). On the other hand, a large fraction of grain boundaries also decreases the electronic conduction (Ref 19). However, some other authors such as Chiang and co-workers (Ref 20) found strongly enhanced electronic conductivity for sintered 1.5 mol.% gadolinium-doped cerium oxide having 10 nm average grain size compared to conventional samples. For higher mol.% of gadolinium, no change in ionic conductivity was measured as function of grain size. In another work by Tuller (Ref 21), conductivity of 5 μm and 10 nm grain-sized CeO_2 were compared at 600 °C. It was demonstrated that under low oxygen partial pressures ($-22 < \log PO_2 < -14$) as the conductivity was electronic, nanostructured CeO_2 showed 104 times higher conductivity. For high PO_2 ($2 < \log PO_2 < 6$), the conductivity of both materials converged. The nano-structured ceria-based thin films have demonstrated a number of great improvements. For example, higher surface area, better coherency, and longer triple phase boundary length (TPBL) compared with the bulk materials. They also provide new opportunity and feasibility for IT-SOFCs commercialization (Ref 22).

Lu Jia and **François Gitzhofer**, Energy, Plasma and Electrochemistry Research Centre (CREPE), Chemical and Biotechnical Engineering Department, Université de Sherbrooke, Sherbrooke, QC J1K 2R1, Canada. Contact e-mail: francois.gitzhofer@usherbrooke.ca.

Thin layers of SOFCs electrolyte have been produced by a number of deposition techniques, including aerosol-assisted metal-organic chemical vapor deposition (MOCVD), polarized electrochemical vapor deposition (PEVD), RF magnetron sputtering, atomic layer deposition (ALD), screen printing, slurry coating, and the sol-gel process (Ref 19, 23-28). These techniques are generally expensive in both equipment and operation costs, and are of rather low efficiency, which makes them difficult to scale up for commercialization. Recently, the plasma spray processes, such as atmospheric plasma spraying, vacuum plasma spraying, low pressure plasma spraying, hybrid plasma spraying, and high velocity oxy-fuel spraying have been developed and adapted to specific requirements of electrolyte deposition in a consecutive and cost-effective spray process (Ref 29-33). However, they suffer from a relatively high coating thickness (50-100 μm), residual porosity/defects (consequently, a post-thermal treatment or an interlayer is needed to seal the anode), and thermal stresses which lack the capability to deposit comparable thin and dense homogenous SOFC electrolytes.

As a promising extension of conventional thermal spraying, the use of a liquid precursor permits feeding and spraying of either metal precursor solutions or a suspension of nano or submicro-sized particles to form thin coatings with more refined microstructure and grain size. The former is known as solution plasma spraying (SolPS) while the latter is known as suspension plasma spraying (SPS). The use of a solution precursor was first reported as a coating technology by Karthikeyan and coworkers (Ref 34, 35). In the SolPS process, solution feedstocks of desired resultant materials are injected into the plasma jet either by atomization or by a liquid stream. Rapid heating and evaporation of solution droplets result in the formation of the solid particles, which are heated and accelerated to the substrate to generate coatings (Ref 36). The as-deposited coatings have the desired porosity. Its' microstructure has nano- and sub-micrometric features (Ref 37-43). SPS, the new method for preparing nano-structured coatings was invented in the mid-1990s by Université de Sherbrooke (Ref 44). In this process, a suspension of micro- or nano-powders is fed to an RF (Ref 45, 46) or to a DC (Ref 47-50) plasma torch and axially or radially injected into the plasma flame (Ref 51, 52). The solid particles enclosed in each droplet are accelerated, evaporated (solvent), melted (solid particles), and then flattened onto a prepared substrate rapidly forming thin (5-10 μm) coatings with a more refined microstructure. Moreover, the composition of applied spray materials can be varied very easily.

In this contribution, the results of SolPS and SPS using inductively coupled thermal plasma for the deposition of dense and thin nano-structured gadolinia-doped ceria (GDC) electrolyte coatings (4-10 μm thick) are presented. The corresponding produced electrolyte layers were characterized and compared to illustrate the correlation between deposition techniques and electrolyte microstructure. In the following sections, the experimental facilities will be presented first. The preparation of the electrolyte powder, of the solution and of the suspension will then be described, as well as the plasma spraying setup. In the third section, the characterization of the injection of the suspension/solution and the interactions of the plasma-particles will be discussed. Finally, the morphologies and microstructures of GDC coatings produced by SolPS and SPS will be compared.

2. Experimental

2.1 Powder Preparation

Electrolyte powders of $Ce_{0.8}Gd_{0.2}O_{1.9}$ (GDC) were prepared by the glycine-nitrate process (GNP) method (Ref 53). Stoichiometric amounts of $Ce(NO_3)_3{\cdot}6H_2O$ (Alfa Aesar, 99.99%) and $Gd(NO_3)_3{\cdot}6H_2O$ (Alfa Aesar, 99.99%) were dissolved in distilled water, to which 0.5 mol glycine per mole nitrate was added. Combustion of the metal nitrate-glycine solution was performed in a glass beaker on a hotplate, with about 20 mL of the solution (0.1 mol with respect to metal ions) burned at a time. The precursor solution turned to a brown-red gel as the solvent was evaporated and then spontaneous combustion occurred, leading to pale-yellow ash. The resultant ash was then collected and calcined in air at 600 °C for 2 h to remove any carbon residues remaining in the oxide powder.

2.2 Solution Precursor Preparation

The solution precursor of GDC was prepared by dissolving separately cerium nitrate hexahydrate (Alfa Aesar, purity: 99.99%) and gadolinium nitrate hexahydrate (Alfa Aesar, purity: 99.99%) in distilled water according to stoichiometric compositions. The solution concentration was 0.6 g/mL. A magnetic stirrer was used to fully mix the starting precursors.

2.3 Suspension Precursor Preparation

To prepare the GDC suspension, GNP-GDC powders were directly dispersed into ethanol. The weight ratio of GDC to ethanol was set to 10%. The suspension viscosity was adjusted by adding Darvan No. 7 (dispersing agent, R.T. Vanderbilt Company, Inc., Norwalk, CT) into the suspension. The mass percentage of the dispersing agent selected for use was 2% of the GDC powder mass to obtain the lowest viscosity for adequate feeding. Before deposition, the suspension mixture was ultrasonically dispersed to break apart the large agglomerates. During injection, a stirrer was used to prevent particles from settling.

2.4 Plasma Spraying Setup

The induction plasma spraying system consisted of a liquid precursor feeder system (Cole-Parmer Canada Inc., Montreal, QC, Canada), an atomization probe (Tekna Plasma Systems Inc., Sherbrooke, QC, Canada), a plasma torch and a plasma reactor. Figure 1 shows the schematic

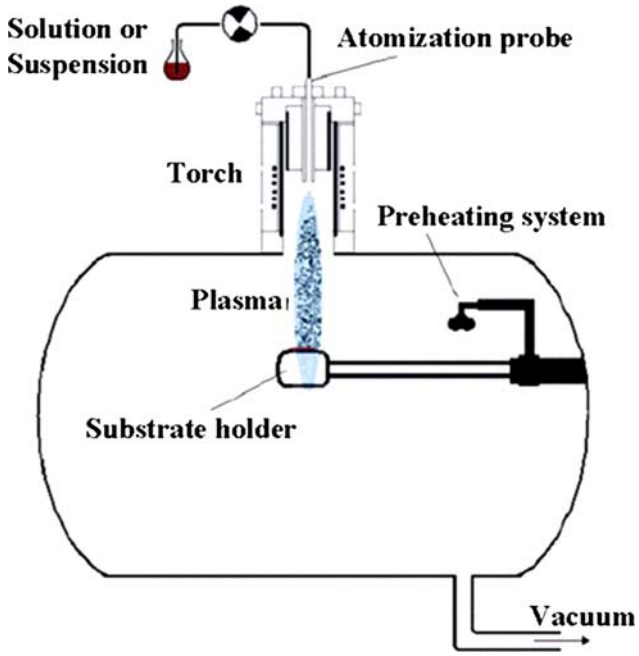

Fig. 1 Schematic illustration of induction plasma system

Table 1 Induction plasma spraying parameters

Plasma torch	Tekna PL-50
Central plasma gas flow rate, slpm	27 (Ar)
Sheath plasma gas flow rate, slpm	80 (O_2)
Plasma power, kW	35-50
Reactor pressure, kPa	6 and 12
Atomization gas pressure, kPa	345 (Ar)
Atomization gas flow rate, slpm	21 (Ar)
Solution injection flow rate, mL/min	10
Suspension injection flow rate, mL/min	4
Spraying distance, mm	100-220

illustration of an induction plasma system. The induction plasma was generated using a PL-50 plasma torch (Tekna Plasma Systems Inc.), operating at a frequency of 3 MHz. The torch is equipped with a supersonic nozzle (diameter = 24.2 mm), in order to increase the plasma velocity (Ref 54). The liquid precursors such as solution or suspension were fed by a peristaltic pump and directly injected into the hot plasma core by means of an atomization probe, resulting in the formation of a coherent deposit. Detailed description of the induction plasma spraying apparatus used for this study is available elsewhere (Ref 54). Table 1 shows the spraying parameters that were used for the synthesis of the electrolytes. The RF power was varied in the range of 35-50 kW, the chamber pressure adjusted at 8 and 12 kPa, and spraying distance was varied from 100 to 220 mm. The atomization parameters were adjusted according to the droplet size measurements using the Malvern RTsizer (Malvern Instruments Limited, Worcestershire, UK) apparatus. The average droplet size (D_{50}) was about 12 μm as measured during water atomization testing.

The substrates (10 mm diameter and 1.2 mm thick) were produced by the sintering of pressed 44 wt.% of green nickel oxide (Novamet type F), 48 wt.% of filamentary nickel powder (Novamet 255), and 8 wt.% of nickel powder (Novamet 210) for 1 h at 800 °C. The substrates were fixed on a sample holder while the holder was scanned across the plasma flame by an electromotive arm. Multiple passes were used to build up the coatings. In order to reduce the thermal gradients during deposition and to obtain dense coating (Ref 55), the substrates were heated up to 300 °C prior to coating using an electric heating device.

2.5 Characterization

Different techniques were used to characterize the materials synthesized by the induction plasma process. Particle size distributions were measured using a Malvern Mastersizer 2000 particle analyzer (Malvern Instruments Ltd., Worcestershire, UK). Structural features analysis was conducted by x-ray diffraction (XRD) using an X'Pert Pro MPD x-ray diffractometer (Philips, Eindhoven, the Netherlands). Morphologies and elemental analyses of electrolyte powders and as-deposited electrolyte layers were performed using a field emission scanning electron microscope (FESEM, model S-4700, Hitachi, Tokyo, Japan). Specific surface areas of the electrolyte powders were determined by the BET method, using an Autosorb-1 instrument (Quantachrome, FL). The as-sprayed coatings were cut using a Buehler ISOMET 2000 Precision Saw and then mounted (infiltrated with EPO-KWICK Buehler low viscosity resin using vacuum impregnation). The polishing was carried out on a Buehler ECOMET 3-VARIABLE SPEED GRINDER POLISHER using procedures outlined for thermal sprayed ceramic coatings in Technical notes published by Buehler. These involve polishing on a 45-μm diamond grid followed by cloth polishing with 9 and 3 μm diamond suspensions and a final step of 0.05 μm alumina suspension. The semi-automatic procedures helped increase the reproducibility of polishing cross sections (Ref 56). Coatings porosity was determined by SigmaScan Pro 5, an image analysis software supplied by Systat Software Inc. A sufficient number of pictures were taken at different sample areas, according to the magnification used. A threshold method was used to determine the darker percentage of the picture that directly provided the porosity (Ref 57). Gas permeability was measured according to Darcy's law (Ref 58). Detailed description of the gas permeability measurement apparatus used for this study is available elsewhere (Ref 46).

3. Results and Discussions

3.1 As-Synthesized GNP-GDC Powder Characteristics

Figure 2 depicts the FESEM micrographs of as-synthesized GNP-GDC powders, indicating that the particle is highly porous with a foam-like microstructure.

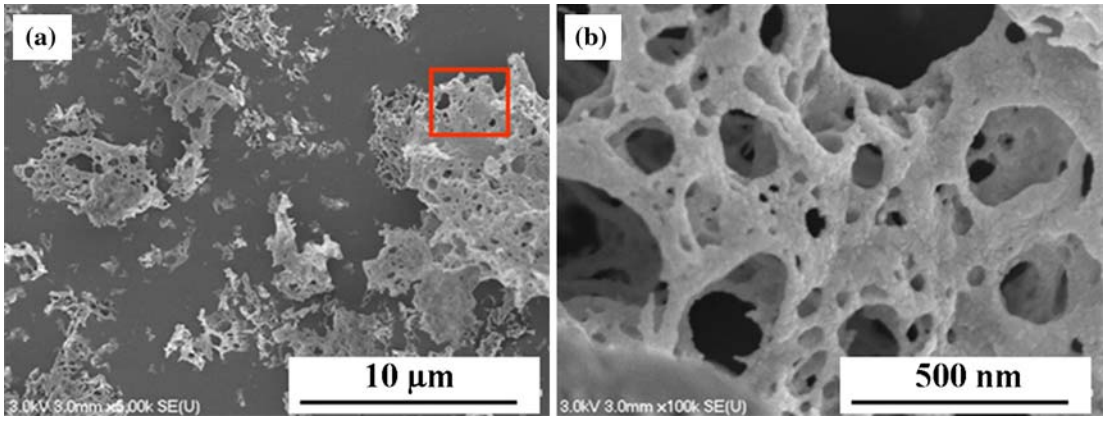

Fig. 2 SEM micrographs of GNP synthesized GDC nano-structured powders with different magnifications

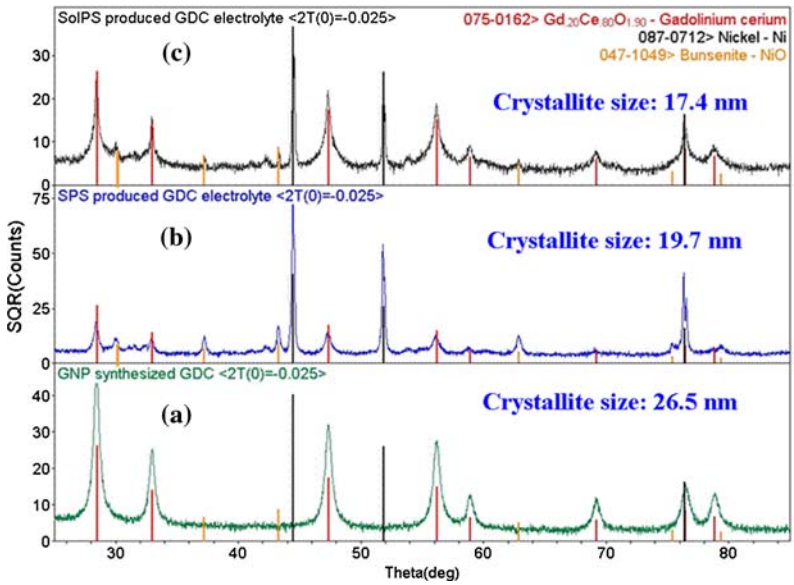

Fig. 3 X-ray analysis for (a) GNP synthesized GDC powders, (b) suspension, and (c) solution plasma-sprayed GDC electrolyte

The XRD pattern (Fig. 3a) of the GNP-GDC sample exhibits all peaks associated with the pure fluorite structure. The crystallite size of the GDC phase, calculated from XRD line-broadening analysis according to the Scherrer equation is 26.5 nm. The specific surface of GDC powders determined by the BET method is 43.1 m^2/g.

Particle sizes distribution of GDC powders elaborated with the GNP technique are shown in Fig. 4. The particle sizes of the GDC powders which ultrasonic treatment was applied for 5 min before the measurement were mostly about 0.6 μm in size with a narrow size distribution. However, before any ultrasonic treatment, the average particle size is 25.5 μm. This is due to porous structures of the agglomerated GDC powders, whose agglomerates were easily broken by the ultrasound. These GDC powders are referred to as weakly agglomerated.

The quality of electrolyte coatings is highly dependent on the size and size distribution of the electrolyte powder particles during suspension preparation and droplet atomization. This is because fine droplets atomized with a narrow size distribution around 12 μm can be evenly plasma treated, resulting in coatings of high homogeneity, high density, and a minimum of flaws.

3.2 Electrolytes Phase Analysis

The x-ray diffraction pattern of the electrolyte shown in Fig. 3(c) indicates that the electrolyte produced by SolPS consists of one highly crystallized phase: GDC. The crystallite size of GDC was calculated from XRD line-broadening analysis according to the Scherrer equation. The crystallite size of GDC for the SolPS coating was estimated to be 17.4 nm. It demonstrates the formation of nano-structured coating, which can enhance the electrocatalytic activity of SOFCs. In addition, traces of NiO and Ni can be identified on the XRD pattern. The NiO and Ni

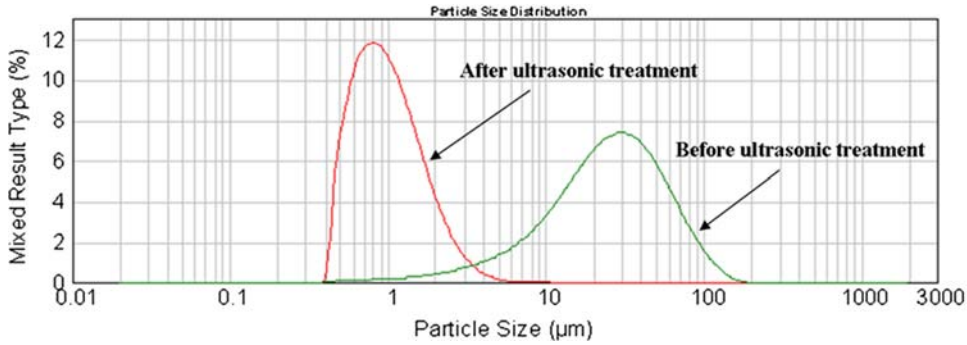

Fig. 4 GNP-GDC particle size distribution (before and after ultrasonic treatment)

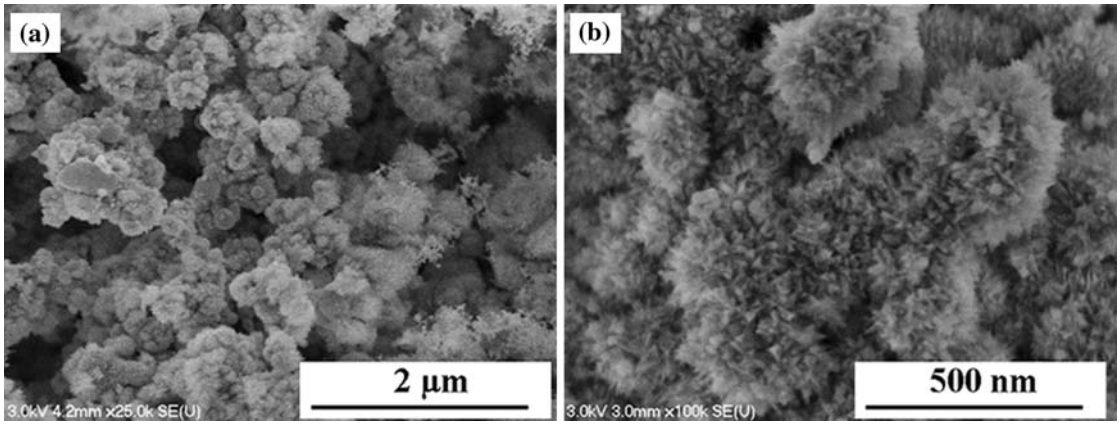

Fig. 5 FESEM micrographs of SolPS produced GDC electrolyte with different magnifications

signals must be collected from the peripheral surface of the substrate. The concentration ratio of Ce and Gd in the precursor solution was chosen in such a way that the crystallite $Ce_{0.8}Gd_{0.2}O_{1.9}$ coatings were to be expected. This indicates the stoichiometric integration of Ce and Gd from the precursor into the coating. This successful synthesis was largely independent of any changes of the process conditions such as plasma power, reactor pressure, plasma gas composition, spraying distance, or substrate temperature. The reason for this ideal stoichiometric behavior might be due to the similar thermodynamic properties of the simple oxides of both elements: Gd_2O_3 and CeO_2 (Ref 14).

The XRD pattern of the electrolytes shown in Fig. 3(b) also indicates that the GDC coatings deposited from suspensions had the same phase content as the initial GDC powders, which implies no major phase transformation during SPS. This is a consequence of the high thermodynamic stability of the solid solutions in the GDC system. The crystallite size of GDC for suspension coating was estimated around 19.7 nm, which is slightly larger than the SolPS-deposited GDC grain size. The difference of the crystallite size in the coatings can be related to the higher plasma temperature associated with a lower fraction of liquid to evaporate for the SPS versus the SolPS, the result being a grain growth associated to a higher plasma heat flux to the substrate.

3.3 Coatings Morphology

Two distinct morphologies of electrolyte coatings deposited by the SolPS processes can be identified by FESEM. Figure 5 shows the micrographs of various magnifications of the coating top surface that was deposited by the SolPS process. The deposit consists of 20 nm size nodule-like particles (Fig. 5b), which were agglomerated into powdery particles. There is an apparent lack of cohesion between different particles. The as-sprayed coatings have rather high porosity. No splats were observed in the SolPS-deposited coatings. The substrate bottom temperature was 400 °C during spraying.

Figure 6 shows FESEM micrographs of multiple splats obtained during SPS depositions. The substrate surface is uniformly covered by the splats. The splats diameter is typically from 0.2 to 2 μm, confirming that coatings obtained by SPS are nano-structured as a typical flattening ratio of 2.7 (Ref 59) results in a splat thickness of 8 to 80 nm nano-structured coatings. Figure 6(b) indicates that the second splat landed on a previously solidified splat and in spite of the perturbations caused by thickness variation

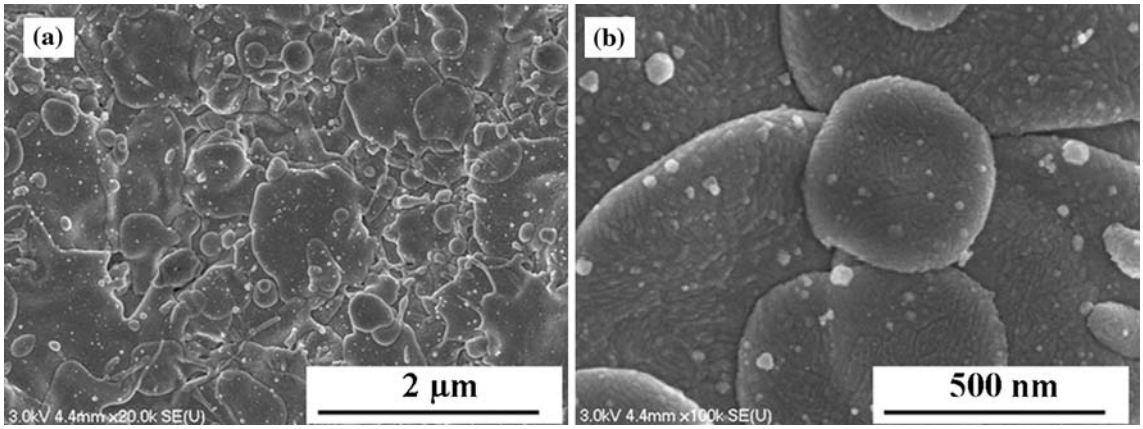

Fig. 6 FESEM micrographs of SPS produced GDC electrolyte with different magnifications

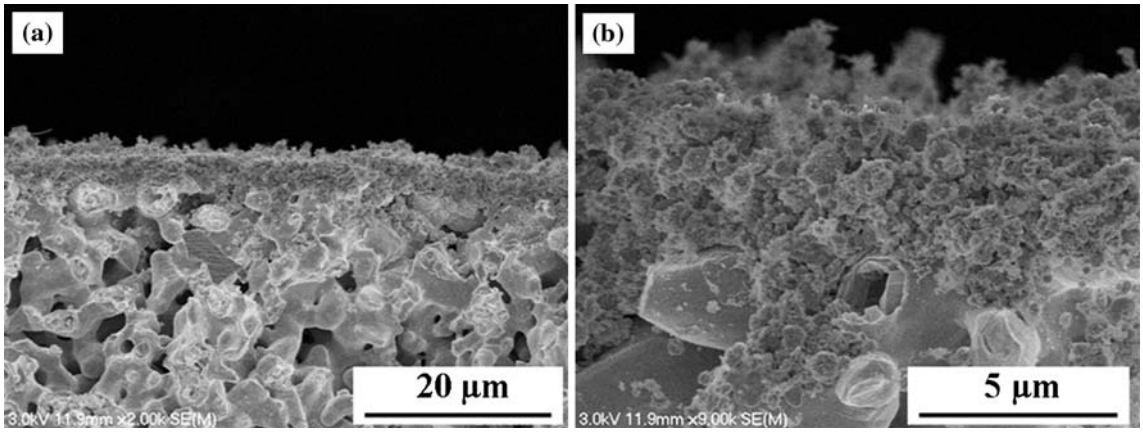

Fig. 7 FESEM micrographs of the fracture cross section of SolPS deposited electrolyte with different magnifications

and roughness, they maintained a relatively contiguous disk-shaped morphology. This suggests that the conventional plasma spray process phenomena (Ref 60) can be used to describe the SPS-deposition process.

Small spherical particles of GDC of about 20 nm were found on the splats (Fig. 6b). This could be due to the extremely high temperature of the induction plasma; the nano-powders in the suspension were vaporized and then condensed onto the coating surface. It was obvious that there was no crack network on the coating surface. This process provides an opportunity to obtain high density and high-sealed electrolytes with thin coatings.

3.4 Coating Microstructure

Figure 7 is the FESEM micrographs of a cross-sectional fracture surface of the SolPS-deposited coatings. It is noted that all coatings deposited from the solution reveal a globular microstructure. The individual particles range in size from about 0.2 to 0.5 μm which suggests that they were formed in flight by homogeneous nucleation from the supersaturated precursor vapors. These coatings seem to be constituted of stacking of small ''particles'', which increases the coating porosity to 7.3% (gas permeability = 3.70×10^{-15} m^2). Previous work demonstrated that a faster plasma jet can dramatically increase the particle impact velocity, which, in conjunction with high particle temperatures, leads to improved flattening of the splats and densification of the coating (Ref 29). A short spray distance (~100 mm) was found to be imperative to produce the dense electrolyte using induction plasma technology (Ref 46). With a low spraying distance of 100 mm and a lower feed rate or a lower concentration, the porosity decreases to about 5.1% (gas permeability = 1.20×10^{-15} m^2), which is still not dense enough for SOFC application without post-treatment. The thickness of the coating measured on the cross section was approximately 5 μm. The higher magnification FESEM micrograph in Fig. 7(b) shows that a good contact can be observed at the interface of sprayed GDC electrolyte and the substrate.

Figure 8(a) and (b) shows the fracture cross section of the SPS-deposited electrolytes. It can be clearly seen that the SPS coating is much more homogeneous and shows better bonding and continuous contact with the Ni substrate compared to the SolPS coating. Figure 8(b)

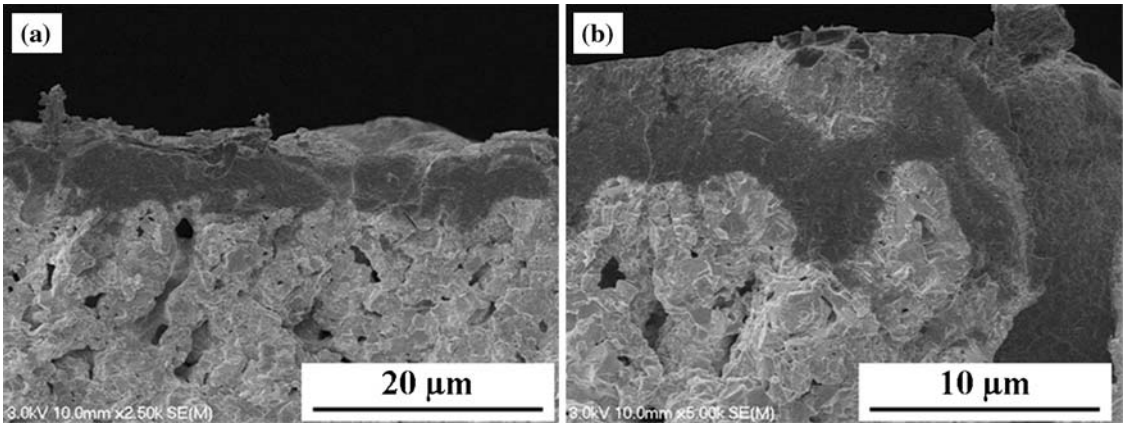

Fig. 8 FESEM micrographs of the fractured cross section of SPS deposited electrolytes

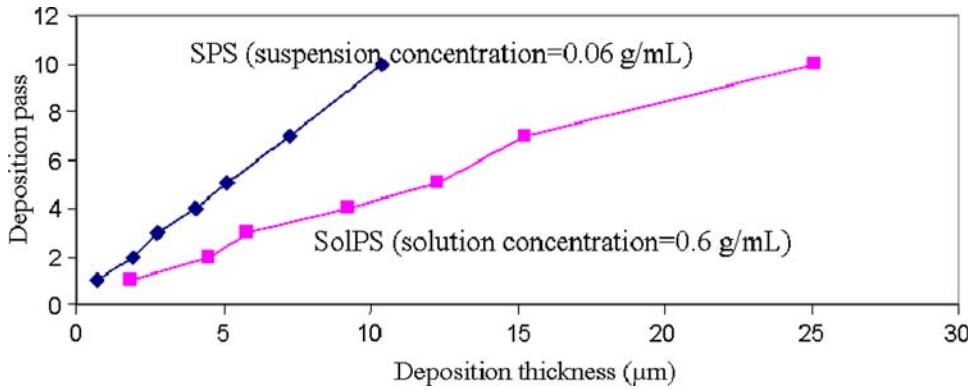

Fig. 9 SolPS/SPS deposition rates

(which is a magnified FESEM photograph of Fig. 8a) illustrates that the GDC layer is very dense. The coating porosity is 1.4% (gas permeability = 0). The distinct interfacial boundary cannot be found between the GDC electrolyte and the substrate. The fine particles of well-dispersed GDC penetrate the pores and cracks of the support and certainly improve the smoothness to enable the formation of the dense GDC top layer. Due to this 3D penetration structure, the adhesion of the interface is improved; there is also an increase in the number of active reaction sites. It is beneficial for the ionic and electronic transfer; thus, it should improve the performance of the films to be used as SOFC electrolyte.

Normally, the electrolyte layer deposited by the conventional plasma spray process is 100-150 μm thick; however, the SPS process is suitable of producing a thin and dense layer of 5 μm in thickness while keeping continuity and uniformity of the coating under the optimized plasma condition. There is also no need of an intermediate layer between the anode and the thin electrolyte as described by Chen et al. (Ref 61).

3.5 Deposition Rates

The thickness of the coatings can be monitored very precisely with a relative easiness thanks to the precursor concentration and the number of deposition passes. Figure 9 presents the dependence of the thickness of GDC films as a function of the number of deposition passes. Considering the coating quality, the solution of 0.6 g/mL and suspension of 0.06 g/mL concentration were used. As it can be seen, the thickness is a linear function of the number of depositions and increases by 1 μm for each SPS pass and 2.5 μm for each SolPS pass, respectively. A small deviation from this relationship is observed for the first two to three passes, which is probably related to the establishment of a continuous film. Taking into account the mass concentration and injection flow rate differences of SolPS and SPS, SPS had an estimated deposition efficiency ten times larger than SolPS.

4. Conclusions and Future Works

In the SolPS process, the solutions completely vaporized in the plasma, and then nano-structured GDC particles were synthesized in flight by homogeneous nucleation from the supersaturated precursor vapor, to subsequently build up a coating with high porosity. The formation of globular GDC coatings was observed over the entire experimental range of this study.

SPS, a highly successful technology was adapted for dense electrolyte deposition. Nano-structured thin-film electrolyte (~5 μm thick) could then be deposited on porous anodes with a high deposition rate. Compared to the electrolytes produced by SolPS, the GDC layer was impervious. These layers were deposited by layering splats. The size of the splats is from 0.2 to 2.0 μm. Three-dimensional penetration structure eliminated the rough surface of the anode and made a much better cohesion between the electrolyte and anode, hence creating longer TPBL, thus improving the electrochemical performance. These results have shown that SPS coating is a simple and potentially commercial technology for preparing the SOFCs electrolytes.

The open circuit voltage of the electrolytes will be measured in the near future, and the single cell will be fabricated and evaluated based on the result of the electrolyte electrochemical measurement. Moreover, in order to investigate the influence of electrolyte microstructure on the electrical conductivity of the electrolyte, single cell with nano-structured electrolyte will be compared to the one with coarse-grained electrolyte according to the electrochemical performance.

Acknowledgments

This project was funded by the Natural Sciences and Engineering Research Council of Canada (NSERC) through strategic grant # STPGP 350705-2007. Furthermore, the help of Doctoral Candidate Tony Rivard in the preparation of GNP-GDC powders is gratefully acknowledged.

References

1. D.T. Hooie, Status of SOFC Development in USA, *Proceed. Electrochem. Soc.*, 1993, **93-94**, p 3-5
2. S.C. Singhal, Science and Technology of Solid-Oxide Fuel Cells, *MRS Bull.*, 2000, **25**(3), p 16-21
3. B.C.H. Steele, Materials for IT-SOFC Stacks 35 Years R&D: The Inevitability of Gradualness, *Solid State Ionics*, 2000, **134**(1-2), p 3-20
4. M.C. Williams, Status of Solid Oxide Fuel Cell Development and Commercialization in the U.S., *Proceed. Electrochem. Soc.*, 1999, **99-19**, p 3-9
5. T. Tsai, E. Perry, and S. Barnett, Low-Temperature Solid-Oxide Fuel Cells Utilizing Thin Bilayer Electrolytes, *J. Electrochem. Soc.*, 1997, **144**(5), p 31-33
6. S.R. Wang, T. Kobayashi, M. Dokiya, and T. Hashimoto, Electrical and Ionic Conductivity of Gd-Doped Ceria, *J. Electrochem. Soc.*, 2000, **147**(10), p 3606-3609
7. B.C.H. Steele, Appraisal of $Ce_{1-y}Gd_yO_{2-y/2}$ Electrolytes for IT-SOFC operation at 500°C, *Solid State Ionics*, 2000, **129**, p 95-110
8. M. Sahibzada, B.C.H. Steele, K. Zheng, R.A. Rudkin, and I.S. Metcalfe, Development of Solid Oxide Fuel Cells Based on a $Ce(Gd)O_{2-x}$ Electrolyte Film for Intermediate Temperature Operation, *Catal. Today*, 1997, **38**, p 459-466
9. Y.P. Xiong, K. Yamaji, T. Horita, N. Sakai, and H. Yokokawa, Hole and Electron Conductivities of 20 mol%-$REO_{1.5}$ Doped CeO_2 (RE = Yb, Y, Gd, Sm, Nd, La), *J. Electrochem. Soc.*, 2004, **151**(3), p A407-A412
10. K. Eguchi, T. Setoguchi, T. Inoue, and H. Arai, Electrical Properties of Ceria-Based Oxides and Their Application to Solid Oxide Fuel Cells, *Solid State Ionics*, 1992, **52**, p 165-172
11. H. Inaba and H. Tagawa, Ceria-Based Solid Electrolytes, *Solid State Ionics*, 1996, **83**, p 1-16
12. V.V. Kharton, F.M.B. Marques, and A. Atkinson, Transport Properties of Solid Oxide Electrolyte Ceramics: A Brief Review, *Solid State Ionics*, 2004, **174**, p 135-149
13. N. Maffei and A.K. Kuriakose, Solid Oxide Fuel Cells of Ceria Doped With Gadolinium and Praseodymium, *Solid State Ionics*, 1998, **107**, p 67-71
14. M. Mogensen, N.M. Sammes, and G.A. Tompsett, Physical, Chemical and Electrochemical Properties of Pure and Doped Ceria, *Solid State Ionics*, 2000, **129**, p 63-94
15. H.J. Park and G.M. Choi, Oxygen Permeability of Gadolinium-Doped Ceria at High Temperature, *J. Eur. Ceram. Soc.*, 2004, **24**(6), p 1313-1317
16. T. Mori, J. Drennan, Y.R. Wang, W.G. Mcphee, and J.G. Li, Nano Structural Features in Rare Earth Doped CeO_2 Electrolytes for Solid Oxide Fuel Cells Application, *Trans. Mater. Res. Soc. Jpn.*, 2004, **29**(5), p 1973-1976
17. J. Maier, Nano-Sized Mixed Conductors (Aspects of Nano-Ionics. Part III), *Solid State Ionics*, 2002, **148**, p 367-374
18. I. Kosacki and H.U. Anderson, Microstructure-Property Relationships in Nanocrystalline Oxide Thin Films, *Ionics*, 2000, **6**, p 294-311
19. B. Zhu, Fast Ionic Conducting Film Ceramic Membranes with Advanced Applications, *Solid State Ionics*, 1999, **119**, p 305-310
20. Y.M. Chiang, E.B. Lavk, and D.A. Blom, Defect Thermodynamics and Electrical Properties of Nanocrystalline Oxides: Pure and Doped CeO_2, *Nanostruct. Mater.*, 1997, **9**, p 633-642
21. H.L. Tuller, Ionic Conduction in Nanocrystalline Materials, *Solid State Ionics*, 2000, **131**, p 143-157
22. B. Zhu, Next Generation Fuel Cell R&D, *Int. J. Energy Res.*, 2006, **30**, p 895-903
23. H.Z. Song, H.B. Wang, S.W. Zha, D.K. Peng, and G.Y. Meng, Aerosol-Assisted MOCVD Growth of Gd_2O_3-Doped CeO_2 Thin SOFC Electrolyte Film on Anode Substrate, *Solid State Ionics*, 2003, **156**(3-4), p 249-254
24. M.A. Haldane and T.H. Etsell, Fabrication of Composite SOFC Anodes, *Mat. Sci. Eng. B Solid-State Mater. Adv. Technol.*, 2005, **B121**(1-2), p 120-125
25. Y. Yoo, Fabrication and Characterization of Thin Film Electrolytes Deposited by RF Magnetron Sputtering for Low Temperature Solid Oxide Fuel Cells, *J. Power. Sour.*, 2006, **160**(1), p 202-206
26. E. Gourba, A. Ringuede, M. Cassir, J. Paeivaesaari, J. Niinistoe, M. Putkonen, and L. Niinistoe, Microstructural and Electrical Properties of Gadolinium Doped Ceria Thin Films Prepared by Atomic Layer Deposition (ALD), *Proceed. Electrochem. Soc.*, 2003, **7**, p 267-274
27. C.Q. Xia, F.L. Chen, and M.L. Liu, Reduced-Temperature Solid Oxide Fuel Cells Fabricated by Screen Printing, *Electrochem. Solid-State Lett.*, 2001, **4**(5), p A52-A54
28. R. Muccillo, E.N.S. Muccillo, F.C. Fonseca, Y.V. França, T.C. Porfirio, D.Z. de Florio, M.A.C. Berton, and C.M. Garcia, Development and Testing of Anode-Supported Solid Oxide Fuel Cells with Slurry-Coated Electrolyte and Cathode, *J. Power. Sour.*, 2006, **156**(2), p 455-460
29. R. Vaβen, D. Hathiramani, J. Mertens, V.A.C. Haanappel, and I.C. Vinke, Manufacturing of High Performance Solid Oxide Fuel Cells (SOFCs) with Atmospheric Plasma Spraying (APS), *Surf. Coat. Technol.*, 2007, **202**, p 499-508
30. G. Schiller, R. Henne, M. Lang, R. Ruckdäschel, and S. Schaper, Development of Vacuum Plasma Sprayed Thin-Film SOFC for Reduced Operating Temperature, *Fuel Cells Bull.*, 2005, **21**, p 7-12
31. A. Refke, H.M. Hoehle, and M. Gindrat, New High Efficient Thermal Spray Solution for Perovskite Coatings and Dense Thin Electrolytes Using Triplex Pro-200 APS and LPPS-Thin Film Technology, *ECS Trans.,* 2007, **7**(1), p 339-346
32. T. Yoshida, T. Okada, H. Hamatani, and H. Kumaoka, Integrated Fabrication Process for Solid Oxide Fuel Cells Using Novel Plasma Spraying, *Plasma. Sour. Sci. Technol.*, 1992, **1**(3), p 195-201

33. J.O. Berghaus, J.G. Legoux, C. Moreau, R. Hui, C. Decès-Petit, W. Qu, S. Yick, Z. Wang, R. Maric, and D. Ghosh, Suspension HVOF Spraying of Reduced Temperature Solid Oxide Fuel Cell Electrolytes, *J. Therm. Spray Technol.*, 2008, **17**(5-6), p 700-707
34. J. Karthikeyan, C.C. Berndt, J. Tikkanen, J.Y. Wang, A.H. King, and H. Herman, Preparation of Nanophase Materials by Thermal Spray Processing of Liquid Precursors, *Nanostruct. Mater.*, 1997, **9**, p 137-140
35. J. Karthikeyan, C.C. Berndt, J. Tikkanen, S. Reddy, and H. Herman, Plasma Spray Synthesis of Nanomaterial Powders and Deposits, *Mater. Sci. Eng. A*, 1997, **238**, p 275-286
36. J. Karthikeyan, C.C. Berndt, S. Reddy, J.Y. Wang, A.H. King, and H. Herman, Nanomaterial Deposits Formed by DC Plasma Spraying of Liquid Feedstocks, *J. Amer. Ceram. Soc.*, 1998, **81**(1), p 121-128
37. N.P. Padture, K.W. Schlichting, T. Bhatia, A. Ozturk, B. Cetegen, E.H. Jordan, M. Gell, S. Jiang, T.D. Xiao, P.R. Strutt, E. Garcia, P. Miranzo, and M.I. Osendi, Towards Durable Thermal Barrier Coatings with Novel Microstructures Deposited by Solution-Precursor Plasma Spray, *Acta Mater.*, 2001, **49**, p 2251-2257
38. L. Xie, X. Ma, E.H. Jordan, N.P. Padture, D.T. Xiao, and M. Gell, Identification of Coating Deposition Mechanisms in the Solution-Precursor Plasma-Spray Process Using Model Spray Experiments, *Mater. Sci. Eng. A*, 2003, **362**, p 204-212
39. L. Xie, X. Ma, A. Ozturk, E.H. Jordan, N.P. Padture, B.M. Cetegen, D.T. Xiao, and M. Gell, Processing Parameter Effects on Solution Precursor Plasma Spray Process Spray Patterns, *Surf. Coat. Technol.*, 2004, **183**, p 51-61
40. X.Q. Ma, J.X. Dai, H. Zhang, J. Roth, T.D. Xiao, and D.E. Reisner, Solid Oxide Fuel Cell Development by Using Novel Plasma Spray Techniques, *J. Fuel Cell Sci. Technol.*, 2005, **2**(3), p 190-197
41. F. Gitzhofer, M.E. Bonneau, and M.I. Boulos, Double Doped Ceria Electrolyte Synthesized by Solution Plasma Spraying with Induction Plasma Technology, *Thermal Spray 2001: New Surfaces for a New Millennium*, C.C. Berndt, K.A. Khor, and E.F. Lugscheider, Ed., ASM, Materials Park, OH, 2001, p 61-68
42. R. Henne, Solid Oxide Fuel Cells: A Challenge for Plasma Deposition Processes, *J. Therm. Spray Technol.*, 2007, **16**(3), p 381-403
43. Y. Wang and T.W. Coyle, Solution Precursor Plasma Spray of Nickel-Yittia Stabilized Zirconia Anodes for Solid Oxide Fuel Cell Application, *J. Therm. Spray Technol.*, 2007, **16**(5-6), p 898-904
44. F. Gitzhofer, E. Bouyer, and M.I. Boulos, Suspension Plasma Spray Deposition, U.S. Patent 5,609,921, 1997
45. M. Bonneau, F. Gitzhofer, and M.I. Boulos, SOFC/CeO_2 Doped Electrolyte Deposition, Using Suspension Plasma Spraying, *Thermal Spray: Surface Engineering via Applied Research*, C.C. Berndt, Ed., ASM International, Montréal, QC, Canada, 2000, p 929-934
46. F. Gitzhofer and L. Jia, Induction Plasma Technology Applied to Materials Synthesis for Solid Oxide Fuel Cells, *Int. J. Appl. Ceram. Technol.*, 2008, **5**(6), p 537-547
47. P. Fauchais, R. Etchart-Salas, C. Delbos, M. Tognonvi, V. Rat, J.F. Coudert, and T. Chartier, Suspension and Solution Plasma Spraying of Finely Structured Layer: Potential Application to SOFCs, *J. Phys. D Appl. Phys.*, 2007, **40**, p 2394-2406
48. P. Fauchais, V. Ra, C. Delbos, J.F. Coudert, T. Chartier, and L. Bianchi, Understanding of Suspension DC Plasma Spraying of Finely Structured Coatings for SOFC, *IEEE Trans. Plasma. Sci.*, 2005, **33**(2), p 920-930
49. P. Fauchais, Suspension and Solution Plasma or HVOF Spraying, *J. Therm. Spray Technol.*, 2008, **17**(1), p 1-3
50. R. Rampon, C. Filiatre, and G. Bertrand, Suspension Plasma Spraying of YPSZ Coatings: Suspension Atomization and Injection, *J. Therm. Spray Technol.*, 2008, **17**(1), p 105-114
51. J. Oberste Berghaus, J.-G. Legoux, C. Moreau, R. Hui, and D. Ghosh, Suspension Plasma Spraying of Intermediate Temperature SOFC Components using an Axial Injection DC Torch, *Mater. Sci. Forum*, 2007, **539-543**(2), p 1332-1337
52. K. Wittmann, J. Fazilleau, J.F. Coudert, P. Fauchais, and F. Blein, A New Process to Deposit Thin Coatings by Injecting Nanoparticles Suspensions in a d.c. Plasma Jet, *International Thermal Spray Conference, ITSC 2002*, DVS-Verlag GmbH, Ed., March 4-6, (Essen, Germany), ASM International, 2002, p 519-522
53. C.R. Xia and M.L. Liu, Microstructures Conductivities, and Electrochemical Properties of $Ce_{0.9}Gd_{0.1}O_2$ and GDC-Ni Anodes for Low-Temperature SOFCs, *Solid State Ionics*, 2002, **152-153**, p 423-430
54. L. Jia, C. Dossou-Yovo, C. Gahlert, and F. Gitzhofer, Induction Plasma Spraying of Samaria Doped Ceria as Electrolyte for Solid Oxide Fuel Cells, *Thermal Spray 2004: Advances in Technology and Application*, E. Lugscheider and C.C. Berndt, Ed., ASM International, Osaka, Japan, 2004, p 85-89
55. M. Suzuki, S. Sodeoka, and T. Inoue, Structure Control of Plasma Sprayed Zircon Coating by Substrate Preheating and Post Heat Treatment, *Mater. Trans.*, 2005, **46**(3), p 669-674
56. S. Deshpande, A. Kulkarni, S. Sampath, and H. Herman, Application of Image Analysis for Characterization of Porosity in Thermal Spray Coatings and Correlation with Small Angle Neutron Scattering, *Surf. Coat. Technol.*, 2004, **187**(1), p 6-16
57. M. von Bradke, F. Gitzhofer, and R. Henne, Porosity Determination of Ceramic Materials by Digital Image Analysis—A Critical Evaluation, *Scanning*, 2005, **27**(3), p 132-135
58. M.V. Chor and W. Li, A Permeability Measurement System for Tissue Engineering Scaffolds, *Meas. Sci. Technol.*, 2007, **18**, p 208-216
59. J. Madejski, Solidification of Droplets on a Cold Surface, *Int. J. Heat Mass Trans.*, 1976, **19**(12), p 1351-1356
60. L. Pawlowski, *The Science and Engineering of Thermal Spray Coatings*, Wiley, New York, 1995
61. H.C. Chen, J. Heberlein, and T. Yoshida, Preparation of Films for Solid Oxide Fuel Cells by Center-Injection Low Pressure Plasma Spraying, *Thermal Spray: Meeting the Challenges of the 21st Century*, C. Coddet Ed., May 25-29, (Nice, France), ASM International, 1998, vol. 2, p 1309-1314